Materials Science-Poland, 40(4), 2022, pp. 54-63
http://www.materialsscience.pwr.wroc.pl/
DOI: 10.2478/msp-2022-0047

First-principle study on the effect of S/Se/Te doping and V_{Zn}-H_i coexistence on ZnO electrical conductivity

Yulan Gu[1], Qingyu Hou[1,2,*], Mude Qi[2], Xiang Yin[1], Zhichao Wang[1]

[1]College of Science, Inner Mongolia University of Technology, Hohhot, 010051, PR China

[2]College of Materials Science and Engineering, Inner Mongolia Key Laboratory of Thin Film and Coatings, Inner Mongolia University of Technology, PR China

In a vacuum environment, when ZnO is prepared using the chemical vapor deposition method and the molecular beam epitaxial growth method, H-gap impurities inevitably remain in the ZnO system, which is often ignored. The study of Zn vacancies under experimental conditions poses a challenge. Second, as an n-type semiconductor, ZnO is characterized by a self-compensation of natural donor defects and poor stability, which severely limit the acquisition of p-type ZnO. Based on the above problems, the conductive properties of S/Se/Te doped and V_{Zn}-H_i coexisting ZnO were investigated by first principle to acquire high-stability and high-quality p-ZnO. The study found that $Zn_{35}SO_{35}$, $Zn_{35}SeO_{35}$, and $Zn_{35}SH_iO_{35}$ all have good p-type conductivity, which can effectively improve hole mobility and electrical conductivity. Among them, $Zn_{35}SO_{35}$ has the largest hole concentration at 2.80×10^{21} cm^{-3}, as well as the best conductivity. The choice of $Zn_{35}SO_{35}$ provides a reference for obtaining new high-quality p-type ZnO semiconductors.

Keywords: *ZnO, S/Se/Te doping, H gap, p-type conductivity*

1. Introduction

ZnO exhibits high exciton binding energy (60 meV) [1] and electron mobility [2] at room temperature. It finds wide-ranging applications, including in light-emitting diodes, blue light, UV light-emitting devices [3–5], etc. However, the high resistivity and poor stability of ZnO limit its application in the design of intrinsic ZnO optoelectronic devices, and obtaining high-quality p-type ZnO semiconductors remains a significant challenge [6].

Studies have shown that the valence band top remarkably shifts after doping S/Se/Te in ZnO, which provides a great possibility to achieve the p-ZnO [7]. Experimentally, Niu *et al.* [8] investigated the electrical properties of sulfur on the effect of S/N doped ZnO thin films by radio-frequency (RF) magnetron sputtering. The study showed that p-type semiconductor was actualized in S-doped ZnO. Dib *et al.* [9] investigated the transport properties of the ZnS_xO_{1-x} using the sol–gel method. The results showed that S doping leads to a large increase in the charge carrier concentration in the ZnO system. When $x = 0.1$, the maximum charge concentration of acceptor carriers is $N_A = 2.139\times10^{22}$ cm^{-3} and the mobility $\mu = 16.2610\times10^{-10}$ cm$^2\cdot$V$^{-1}\cdot$s^{-1}. Cai *et al.* [10] studied the p-type conductivity of Se–N co-doped ZnO films by RF magnetron sputtering. The study indicated that under the same growth and annealing conditions, ZnO:N has n-type conductivity, whereas ZnO:Se-N has p-type conductivity, and the hole concentration reaches 4×10^{-16} cm^{-3}. Tang *et al.* [11] investigated the p-type conductivity of N single-doped and Te–N co-doped ZnO by metal-organic chemical vapor deposition (MOCVD). It is found that the hole carrier concentration of the Te–N co-doped ZnO is remarkably higher than that of N-doped ZnO. Park *et al.* [12] investigated the p-type conductivity of Te–N co-doped ZnO system by molecular beam epitaxy. It is found that N-doped ZnO exhibits n-type, whereas Te–N co-doped ZnO transforms to p-type, and the hole concentration reaches 4×10^{-16} cm^{-3}.

Theoretically, Persson *et al.* [13] used the first-principle approaches to study the effect of p-type

* E-mail: qingyu1119@126.com

© Gu *et al.* 2022. This is an open access article distributed under the Creative Commons Attribution-NonCommercial-NoDerivatives 4.0 License. (http://creativecommons.org/licenses/by-nc-nd/4.0/)

ZnO in the $ZnO_{1-x}S_x$ system. The results showed that S doping leads to a remarkable upward shift in the valence band top of ZnO and a decrease in bulk ionization energy, which improves the doping efficiency and stability of p-type ZnO. Hou *et al.* [14] used the first-principle approaches to investigate the effect of triaxial strain on the p-type conductivity of a ZnO (S, Se, Te) system. The research showed that the $Zn_{36}RO_{35}$ (R = S/Se/Te) systems exhibit p-type conductivity, and the hole mobility increases when −5% compressive strain is applied. There are relatively few theoretical calculations from the literature dealing with the effect of S/Se/Te doped ZnO on electrical conductivity.

Some progress has been made in the study of S/Se/Te doping on the p-type conductivity of ZnO, which can solve the bottleneck problem that severely limits the p-type conductivity of ZnO [6–14]. While there are studies in the literature (such as those of Liu *et al.* [15] and Zeng *et al.* [16]) delving into the benefits that a Zn vacancy (V_{Zn}) can bring in terms of enabling ZnO to achieve p-type conductivity, these, for the most part, lack theoretical calculations.. Second, previous experimental studies [7–14] have ignored the fact that in the process of semiconductor preparation, when the chemical vapor deposition method and the molecular beam epitaxial growth method are used in the vacuum environment, the H-gap impurities will inevitably remain in the ZnO matrix [17]. The study of V_{Zn} under experimental conditions poses a challenge. Therefore, it is necessary to systematically study the effects of equivalent element S/Se/Te doping and V_{Zn}–H gap (H_i) on the electrical conductivity of ZnO. Hence, this research has practical importance and academic value.

2. Model construction and calculation model

2.1. Model construction

This paper is based on the hexagonal wurtzite structure of ZnO with symmetry C_{6V}^4. The construction of pure $Zn_{36}O_{36}$ supercell is shown in Figure 1A. This paper considered the unipolarity of ZnO in the z-axis direction and is thus asymmetric. Therefore, the selected doping atomic positions are different, and the stability of the ZnO system is also different. Therefore, a $Zn_{35}RO_{35}$ (R = S/Se/Te) model was constructed, in which the R (R = S/Se/Te) atoms that replaced O atoms and Zn vacancies coexisted, three different substitution positions of R (R = S/Se/Te) atoms were selected from near to far with the relative V_{Zn} as the center and were denoted by a1, a2, and a3, respectively, and the fixed V_{Zn} positions were (0.444, 0.556, 0.500) as shown in Figure 1B. The influence of H_i at different positions on the stability of the ZnO system was studied with consideration of practical factors. From the relative V_{Zn} center from near to far, three doping positions of H_i were considered using b1 (0.700, 0.500, 0.400), b2 (0.763, 0.532, 0.289), and b3 (0.879, 0.591, 0.162), respectively. Then the model of $Zn_{35}RH_iO_{35}$ (R = S/Se/Te) was constructed, as shown in Figure 1C. The doping amounts of S/Se/Te in the model constructed in this paper (1.39 mol%) are lower than the doping amount without phase transition used in the experiments carried out in several comparable studies in the literature [18–20]. The V_{Zn} content in this paper is 2.78 mol%, which is much lower than the V_{Zn} content of 9 mol% used in the experiments comprised in the studies of Wu *et al.* [21] and Ghosh *et al.* [22], and does not cause a phase change in the system. Therefore, the doping amount used in this study is feasible.

2.2. Calculation model

This paper uses the CASTEP (8.0) module in MS for calculations. Based on density functional theory (DFT) [23], generalized gradient approximation (GGA) was adopted [24], and the plane wave supersoft pseudopotential method based on Perdew–Burke–Ernzerhof (PBE) functional was selected [25]. The plane wave cutoff energy was set to 340 eV. The effect of different cutoff energies on the energy convergence of undoped $Zn_{36}O_{36}$ was tested. Figure 2 indicates that when the cutoff energy reaches 340 eV, the energy of the system converges and tends to be stable, and so the choice of a cutoff energy of 340 eV used in this paper may be said to be reasonable. This is con-

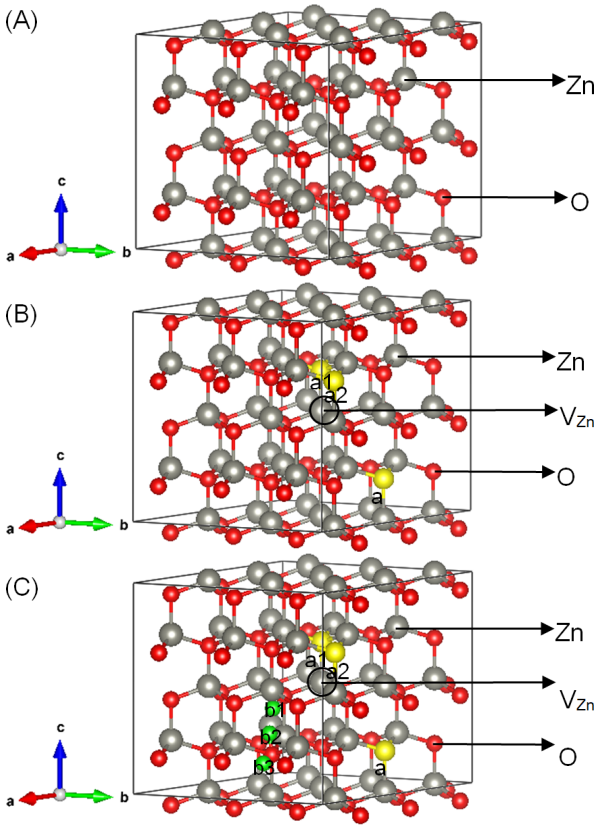

Fig. 1. Model: **(A)** $Zn_{36}O_{36}$, **(B)** $Zn_{35}RO_{35}$ (R = S/Se/Te), and **(C)** $Zn_{35}RH_iO_{35}$ (R = S/Se/Te).
Gray, red, yellow, and green represent Zn, O, R (R = S/Se/Te), and H atoms, respectively

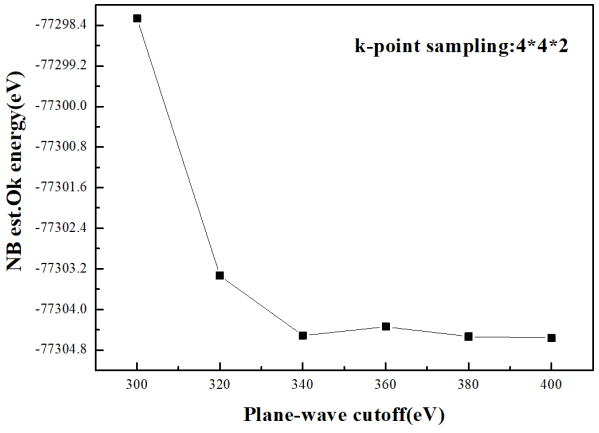

Fig. 2. Relationship between total energy of $Zn_{36}O_{36}$ and cutoff energy

sistent with previous calculations of the energy cutoff radius [26, 27]. The k point sampling of the first Brillouin zone was 4×4×2. The maximum interatomic force, maximum internal stress, and tolerance shift convergence accuracy were 0.01 eV·Å^{-1}, 0.02 GPa, and 0.0005 Å, respectively. The electron density is not spin polarized, and the charge was set to values adapted to a given case. The valence electron configuration of each atom is: S–$3s^2 3p^4$, Se–$4s^2 4p^4$, Te–$5s^2 5p^4$, Zn–$3d^{10} 4s^2$, O–$2s^2 2p^4$, and H–$1s^1$.

3. Results and discussion

3.1. Crystal structure, formation energy, and stability analyses

The doped $Zn_{36}O_{36}$, $Zn_{35}RO_{35}$ (R = S/Se/Te), and $Zn_{35}RH_iO_{35}$ (R = S/Se/Te) systems were geometrically optimized, and the optimized results are listed in Table 1. The calculated lattice constants of the $Zn_{36}O_{36}$ system are in good agreement with the experimental values of $a = b = 3.258$ Å and $c = 5.220$ Å [28]. The rationality underlying the choice of parameters employed in this study is verified.

Table 1 showed that the a, c, and V of $Zn_{35}RO_{35}$ (R = S/Se/Te) and $Zn_{35}RH_iO_{35}$ (R = S/Se/Te) were larger than those of $Zn_{36}O_{36}$. One reason for this finding is attributable to the radius effect: the S/Se/Te ionic radius (2.14/2.24/2.42 Å) [29] is larger than the O ionic radius (1.71 Å) [29]. The second reason is the interionic force: the repulsive force between V_{Zn} and O, R (R = S/Se/Te) is greater than the attractive force between V_{Zn} and Zn in the $Zn_{35}RO_{35}$ (R = S/Se/Te) systems; the repulsive forces between H and V_{Zn}, between V_{Zn} and O, and between V_{Zn} and R (R = S/Se/Te) are greater than the attraction force between O and H, V_{Zn} and H, and H and R (R = S/Se/Te) in the $Zn_{35}RH_iO_{35}$ (R = S/Se/Te) systems. Therefore, the volume of the $Zn_{35}RO_{35}$ (R = S/Se/Te) and $Zn_{35}RH_iO_{35}$ (R = S/Se/Te) systems increases. Table 1 shows that compared with the $Zn_{35}RO_{35}^{a2-a3}$ (R = S/Se/Te) and $Zn_{35}RH_iO_{35}^{a2-a3}$ (R = S/Se/Te) systems, when the relative distance between the R (R = S/Se/Te) substitution atom and V_{Zn} is closest to 1.992 Å, the increase in the equivalent unit cell volume caused by doping can be reduced, improv-

Table 1. Relative distance d between the replacement atoms and V_{Zn}; the reduced lattice constants a and c and volume V of $Zn_{36}O_{36}$, $Zn_{35}RO_{35}$ (R = S/Se/Te)$^{a1-a3}$, and $Zn_{35}RH_i^{b1-b3}O_{35}^{a2}$ (R = S/Se/Te) doping systems

Models	$d_{M\text{-}V_{Zn}}$ (Å)	a (Å)	c (Å)	V (Å^3)
$Zn_{36}O_{36}$	–	a = 3.287	c = 5.299	49.485
$Zn_{35}SO_{35}^{a1}$	1.992	a = 3.301	c = 5.298	49.988
$Zn_{35}SO_{35}^{a2}$	3.811	a = 3.303	c = 4.955	50.490
$Zn_{35}SO_{35}^{a3}$	4.570	a = 3.303	c = 5.334	50.385
$Zn_{35}SeO_{35}^{a1}$	1.992	a = 3.304	c = 5.294	50.047
$Zn_{35}SeO_{35}^{a2}$	3.811	a = 3.307	c = 5.351	50.708
$Zn_{35}SeO_{35}^{a3}$	4.570	a = 3.307	c = 5.338	50.584
$Zn_{35}TeO_{35}^{a1}$	1.992	a = 3.308	c = 5.295	50.204
$Zn_{35}TeO_{35}^{a2}$	3.811	a = 3.316	c = 5.373	51.131
$Zn_{35}TeO_{35}^{a3}$	4.570	a = 3.315	c = 5.344	50.927
$Zn_{35}SH_i^{b1}O_{35}^{a1}$	1.992	a = 3.307	c = 5.316	50.332
$Zn_{35}SH_i^{b2}O_{35}^{a1}$	1.992	a = 3.332	c = 5.289	50.427
$Zn_{35}SH_i^{b3}O_{35}^{a1}$	1.992	a = 3.314	c = 4.968	50.546
$Zn_{35}SeH_i^{b1}O_{35}^{a1}$	1.992	a = 3.309	c = 5.316	50.402
$Zn_{35}SeH_i^{b2}O_{35}^{a1}$	1.992	a = 3.334	c = 5.286	50.468
$Zn_{35}SeH_i^{b3}O_{35}^{a1}$	1.992	a = 3.316	c = 5.317	50.607
$Zn_{35}TeH_i^{b1}O_{35}^{a1}$	1.992	a = 3.317	c = 5.322	50.620
$Zn_{35}TeH_i^{b2}O_{35}^{a1}$	1.992	a = 3.345	c = 5.293	50.690
$Zn_{35}TeH_i^{b3}O_{35}^{a1}$	1.992	a = 3.325	c = 5.322	50.825

ing the stability of the structure. This outcome was further confirmed by the formation energies.

The formation energies of all the doped systems were calculated to analyze the stability of doped systems. The calculation formula is expressed as the following in the literature [30, 31]:

$$E_f(R+V_{Zn}) = E_{ZnO:R+V_{Zn}} - E_{ZnO} - \mu_R + \mu_O + \mu_{Zn} \quad (1)$$

$$E_f(R+V_{Zn}+H_i) = E_{ZnO:R+V_{Zn}+H_i} - E_{ZnO} - \mu_R - \mu_{H_i} + \mu_O + \mu_{Zn} \quad (2)$$

where $E_{ZnOR+V_{Zn}}$ represents the total energy of the ZnO:V_{Zn}+R (R = S/Se/Te) system; $E_{ZnOR+V_{Zn}+H_i}$ is the total energy of the ZnO:V_{Zn}+H_i+R (R = S/Se/Te) system; E_{ZnO} represents the total energy of the pure $Zn_{36}O_{36}$ system; and μ_R, μ_{Hi}, μ_O, and μ_{Zn} are the chemical potentials of S/Se/Te atom, H atom, O atom, and Zn atom, respectively. $\mu_{ZnO}(bulk) = \mu_O + \mu_{Zn}$; thus, μ_O and μ_{Zn} were included in the calculation formula of the E_f of the doped system. The E_f of the system were the same in O- and Zn-rich conditions; hence, this paper did not separately calculate the E_f in O- and Zn-rich conditions. The E_f calculation results are shown in Figure 3. According to Figure 3, among the $Zn_{35}RO_{35}$ (R = S/Se/Te) systems, the $Zn_{35}SO_{35}$ system had the lowest formation energy and was relatively stable. This result is attributable to the fact that among the three dopant atoms of S, Se, and Te, the radii of S and O atoms were the closest, the lattice distortion caused by the substitution of S atom for O atom was the smallest, and the structure was the most stable. In $Zn_{35}RO_{35}^{a1-a3}$ (R = S/Se/Te), when the R replacement atom was closest to V_{Zn} (1.992 Å), the E_f of the $Zn_{35}RO_{35}^{a1}$ (R = S/Se/Te) was the most stable system.

The system with the lowest formation energy in the $Zn_{35}RH_iO_{35}$ (R = S/Se/Te) system was selected, and the formation energies of the b1, b2, and b3 positions of the H_i were calculated to explore the effect of the H_i position on the stability of the ZnO. The results are shown in Figure 4. The figure shows that the E_f of the $Zn_{35}RH_iO_{35}$ (R = S/Se/Te) system also increased gradually with the increase in the distance between H_i and V_{Zn}. The formation energy of the $Zn_{35}RH_i^{b1}O_{35}^{a1}$ (R = S/Se/Te) system

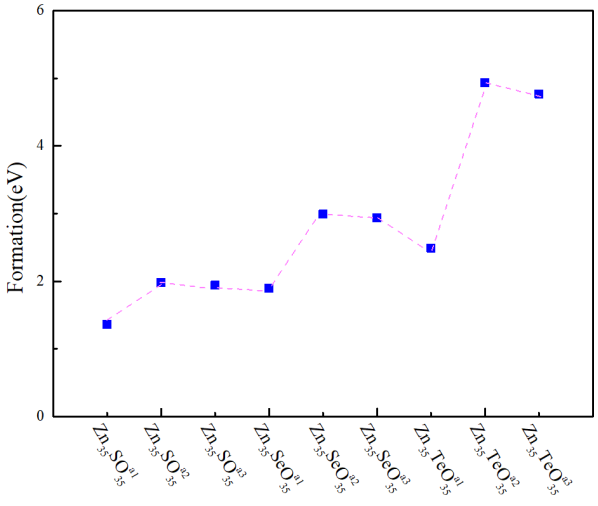

Fig. 3. Formation energies of $Zn_{35}RO_{35}^{a1-a3}$ (R = S/Se/Te) systems with different relative distances between R substitution atoms and V_{Zn}

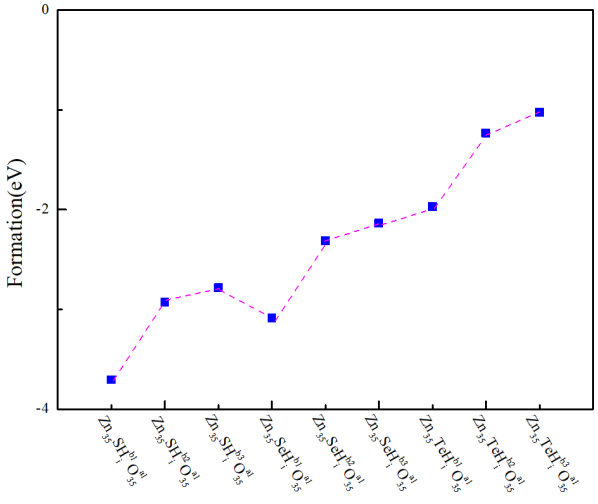

Fig. 4. Formation energies of the $Zn_{35}RH_i^{b1-b3}O_{35}^{a1}$ (R = S/Se/Te) system with different positions of b1, b2, and b3 in the H_i

was the lowest when H_i was located at the b1 position, which is the nearest neighbor center position, because V_{Zn} was the acceptor, and a Coulomb attraction was present between it and the donor H_i. A closer distance corresponds to a more stable system. This result is consistent with a similar research [32].

Considering the structural stability of the system, the most stable $Zn_{35}RO_{35}^{a1}$ (R = S/Se/Te) and $Zn_{35}R^{b1}H_iO_{35}^{a1}$ (R = S/Se/Te) systems were selected as the research objects. The superscripts of the above systems were omitted to facilitate subsequent research.

3.2. Mobility analysis

Mobility is an important parameter used to measure the conductivity of a system. The p-type conductivity of the system is proportional to the hole mobility. A higher hole mobility indicates that the p-type conductivity of a system is better. The hole mobility formula [33, 34] is:

$$\mu_h^{3D} = \frac{2^{3/2}\pi^{1/2}}{3}\frac{c^{3D}\hbar^4 e}{E_I^2 m_h^{*5/2}(k_B T)} \tag{3}$$

where c^{3D} is the elastic modulus, defined as $c^{3D} = \frac{\left[\frac{\partial^2 E}{\partial \delta^2}\right]}{V_0}$ [35], E is the total energy of the system, and V_0 is the total volume of the system at equilibrium. E_I is the deformation potential energy, defined as $E_I = \frac{\Delta E}{\delta}$ [34], where δ is the deformation amount, and ΔE is the energy change at the top of the valence band along the transport direction. m_h^* is the effective mass of the hole, defined as $m^* = \hbar^2\left(\frac{d^2E}{dk^2}\right)^{-1}$, where m^* is the effective mass of the carrier, $\hbar$ is Planck's constant, k is the direction of the wave vector, and E is the energy of the carrier in the wave vector k. T is the temperature, which was set to 300 K. The smaller the m_h^* of the holes and the smaller the E_I, the greater the system mobility and the better the electrical conductivity. The calculated data of each system according to Eq. (3) are shown in Table 2. The calculated effective mass of pure $Zn_{36}O_{36}$ was consistent with the experimental value ascertained in the study of Janotti *et al.* [36], which shows that the data in this paper are reliable.

Table 2 shows that the hole mobilities of the $Zn_{35}RO_{35}$ (R = S/Se/Te) and $Zn_{35}RH_iO_{35}$ (R = S/Se/Te) systems are anisotropic. This result is attributable to the fact that ZnO has unipolarity, and therefore, the mobility of the system is different along different transport directions. In the $Zn_{35}RO_{35}$ (R = S/Se/Te) and $Zn_{35}RH_iO_{35}$ (R = S/Se/Te) systems, the hole mobilitiy of the $Zn_{35}SO_{35}$ system along the a-axis was the highest,

Table 2. Effective mass, elastic modulus, deformation potential, and hole mobility of $Zn_{35}RO_{35}$ (R = S/Se/Te) and $Zn_{35}RH_iO_{35}$ (R = S/Se/Te) systems

Models	Direction	$m_h^* \cdot m_o^{-1}$	c^{3D} ($\times 10^{11} J \cdot m^{-2}$)	E_I(eV)	μ_h ($cm^2 \cdot V^{-1} \cdot s^{-1}$)
$Zn_{36}O_{36}$	∥ a	0.22	0	0	0
		0.21 [35]	0	0	0
	∥ c	0.17	0	0	0
		0.24 [35]	0	0	0
$Zn_{35}SO_{35}$	∥ a	6.91	54.17	5.07	103.60
	∥ c	137.89	43.12	4.54	0.058
$Zn_{35}SeO_{35}$	∥ a	35.93	68.79	2.80	6.698
	∥ c	744.99	67.35	2.77	0.004
$Zn_{35}TeO_{35}$	∥ a	7.23	123.73	44.74	2.707
	∥ c	5.06	136.331	46.96	6.625
$Zn_{35}SH_iO_{35}$	∥ a	19.70	82.69	2.96	33.795
	∥ c	10.31	57.79	2.47	170.383
$Zn_{35}SeH_iO_{35}$	∥ a	12.02	95.64	20.54	2.79
	∥ c	2.25	71.01	17.70	183.061
$Zn_{35}TeH_iO_{35}$	∥ a	9.69	118.47	38.63	1.674
	∥ c	1.74	104.50	36.28	122.634

and the hole mobilities of the $Zn_{35}SeH_iO_{35}$ system along the c-axis were the highest. Table 2 displays that in tandem with the unintentional incorporation of H_i, the hole mobility of the doped system decreases along the *a* direction and increases along the *c* direction. The results showed that the unintentional incorporation of the H_i can greatly increase the mobility of the doping system along the *c* direction, but it is not conducive to the mobility along the *a* direction.

3.3. Band analysis

The calculated band structure of pure $Zn_{36}O_{36}$ system is shown in Figure 5. The bandgap of the pure $Zn_{36}O_{36}$ system is 0.73 eV, which is close to the calculated result available from the literature [37], but inconsistent with the experimental value (3.37 eV). This is because the energy of Zn–3*d* is overestimated when the architecture is calculated using GGA, resulting in an underestimation of the bandgap [38]. However, this error has little effect on the analysis of the relative physical quantities of the ZnO system.

The calculated band structures of the $Zn_{35}RO_{35}$ (R = S/Se/Te) and $Zn_{35}RH_iO_{35}$ (R = S/Se/Te) systems are shown in Figures 6A–6F.

According to Figures 6A–6F, the valence band

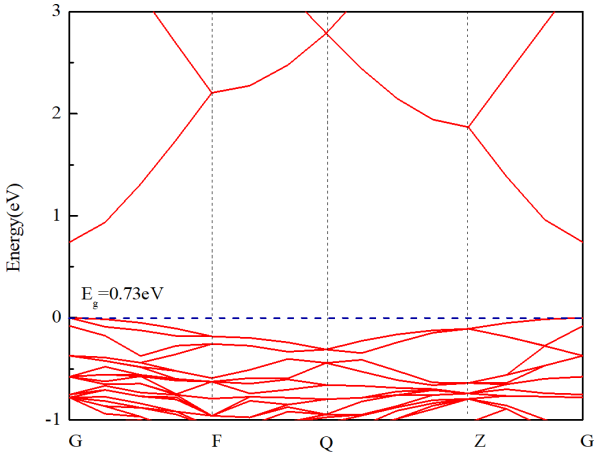

Fig. 5. Band structure of pure $Zn_{36}O_{36}$

maximum (VBM) and conduction band minimum (CBM) of the doped systems correspond to the same high symmetry point, which indicates that they are all direct bandgap semiconductors. The figures indicate that R (R = S/Se/Te) and H_i lead to remarkable changes in the valence and conduction bands of the system. Among them, the VBM and CBM of the $Zn_{35}SO_{35}$, $Zn_{35}SeO_{35}$, and $Zn_{35}SH_iO_{35}$ systems moved up, the Fermi level entered the valence band, and the systems were the p-type semiconductor. However, the VBM and CBM of the $Zn_{35}TeO_{35}$, $Zn_{35}SeH_iO_{35}$, and $Zn_{35}TeH_iO_{35}$

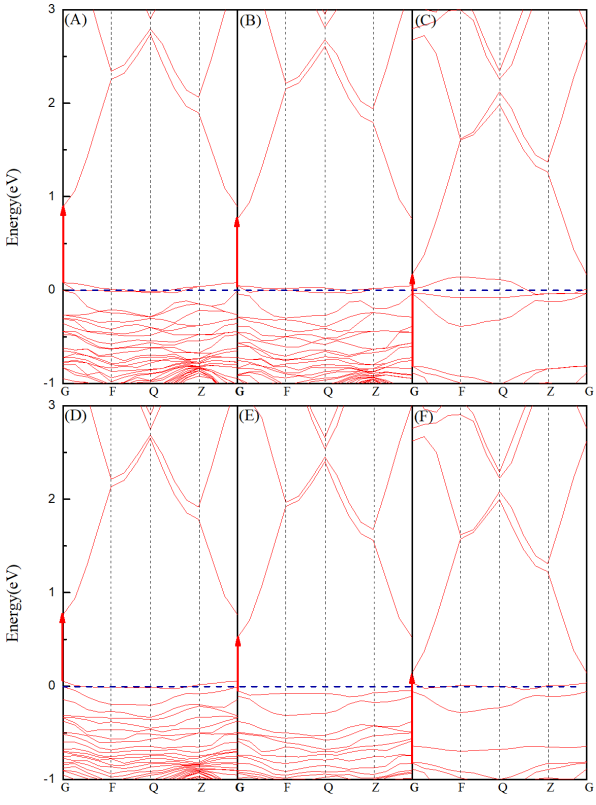

Fig. 6. Band structure distribution: **(A)** $Zn_{35}SO_{35}$; **(B)** $Zn_{35}SeO_{35}$; **(C)** $Zn_{35}TeO_{35}$; **(D)** $Zn_{35}SH_iO_{35}$; **(E)** $Zn_{35}SeH_iO_{35}$; and **(F)** $Zn_{35}TeH_iO_{35}$

systems moved down, and the Fermi level was located between the valence and conduction bands, indicating that no p-type degeneracy had occurred. Therefore, studying the electrical conductivities of the $Zn_{35}TeO_{35}$, $Zn_{35}SeH_iO_{35}$, and $Zn_{35}TeH_iO_{35}$ systems will be meaningless; accordingly, these three systems were not further studied.

3.4. Hole transport characteristics analysis

The total density of states (DOS) and partial density of states (PDOS) of the $Zn_{36}O_{36}$, $Zn_{35}SO_{35}$, $Zn_{35}SeO_{35}$, and $Zn_{35}SH_iO_{35}$ systems were calculated to study the effect of doping defects on the hole concentration of the ZnO system (Figures 7A–7D).

Figures 7A–7D illustrate that the O–2*p* state in the $Zn_{36}O_{36}$ system determines the VBM, and the Zn–4*s* state determines the CBM. Its Fermi level did not enter the valence band and was not a p-type degeneracy semiconductor. The Fermi levels of the $Zn_{35}SO_{35}$, $Zn_{35}SeO_{35}$, and $Zn_{35}SH_iO_{35}$ systems entered the valence band, which indicates that they are all p-type semiconductors. This is consistent with the analysis results in Section 3.3.

Figures 7B and 7C indicate that the upper valence bands of the $Zn_{35}SO_{35}$ and $Zn_{35}SeO_{35}$ systems in the range of −3 eV to 0 eV were formed by the hybridization of O–2*p* and a small amount of Zn–3*d* state orbital. The lower valence band from −6 eV to −3 eV was formed by the hybridization of Zn–3*d* and a small amount of O–2*p* orbitals. The electrons in the O–2*p* and S–3*p*/Se–4*p* states occupy the vicinity of the Fermi level, and *p*–*p* state coupling occurs and the VBM moves up. This is because the atomic number of O group elements increases, which leads to the rise of the *p*-state energy level and the rise of the VBM. The carriers were degenerated, and the system exhibited p-type conductivity. The calculation results showed that S/Se doping is beneficial to the transition of the ZnO system from a natural n-type semiconductor to a p-type semiconductor.

Figure 7D shows that the valence band of the $Zn_{35}SH_iO_{35}$ system was formed by the coupling of O–2*p*, Zn–3*d*, and S–2*p* state orbits. Near the Fermi level, *p*–*p* state coupling occurs between the *p*-state orbital of S and the *p*-state orbital of O, the VBM moves up, and the Fermi level enters the valence band. The reason is the same as above. Notably, Figure 7D shows that the H–1*s* state contributes to the DOS near −7 eV. This result indicates that the doping of H_i affects the low-valence band region and does not contribute much to the electronic states near the Fermi level.

Another reference factor that cannot be ignored when exploring the conductivity of p-type semiconductors is the hole concentration. In this paper, as shown in Figures 7B–7D, Origin 8.5 software was used to integrate the part of the DOS beyond the Fermi level, and the hole concentration P_i is equal to the integral value divided by the total volume of the doped system. The calculation results are shown in Table 3.

Table 3 shows that the hole concentrations of the $Zn_{35}SO_{35}$ and $Zn_{35}SeO_{35}$ systems were con-

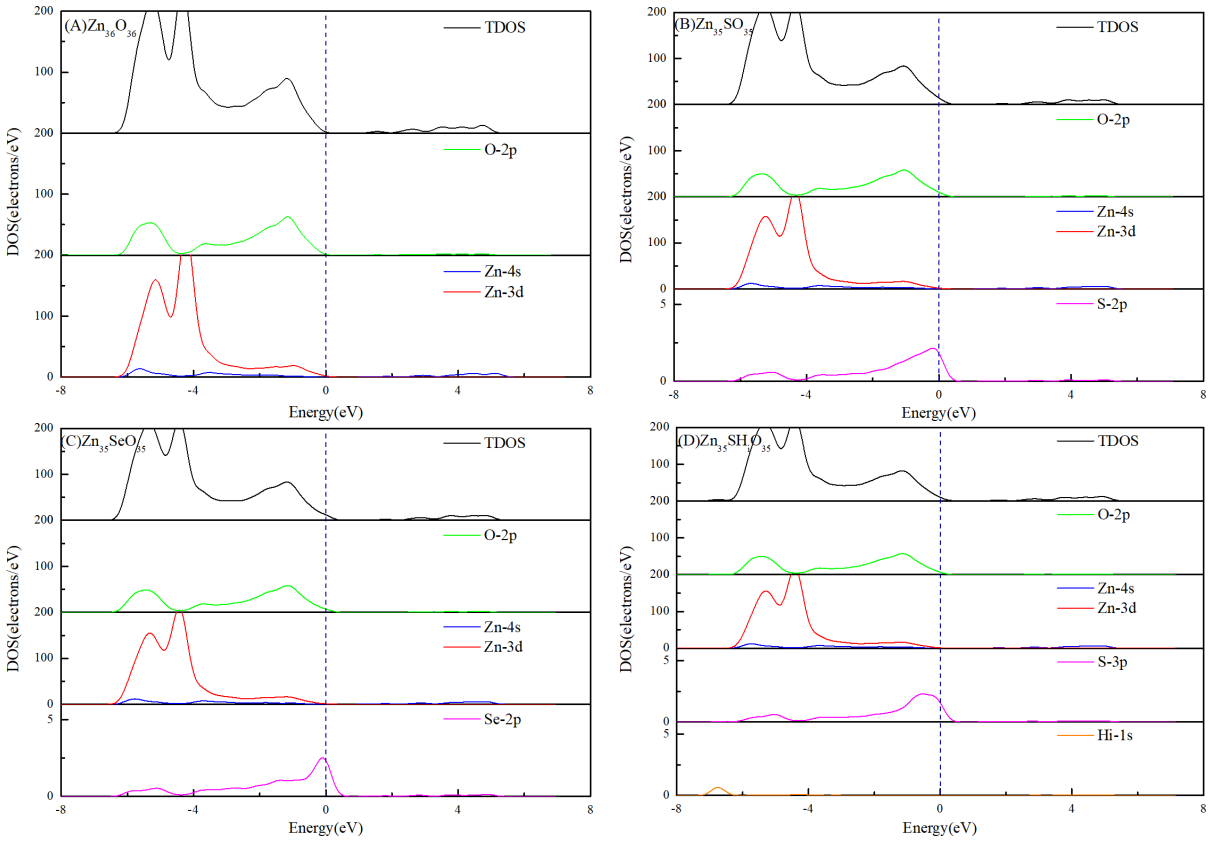

Fig. 7. DOS analysis diagram: **(A)** $Zn_{36}O_{36}$, **(B)** $Zn_{35}SO_{35}$, **(C)** $Zn_{35}SeO_{35}$, and **(D)** $Zn_{35}SH_iO_{35}$. DOS, density of states

Table 3. Hole concentrations of the $Zn_{36}O_{36}$, $Zn_{35}SO_{35}$, $Zn_{35}SeO_{35}$, and $Zn_{35}SH_iO_{35}$ systems

Models	P_i **(×10^{21} cm^{-3})**
$Zn_{36}O_{36}$	0
$Zn_{35}SO_{35}$	2.80
Zn $_{35}SeO_{35}$	2.42
$Zn_{35}SH_iO_{35}$	1.74

siderably higher than that of the $Zn_{35}SH_iO_{35}$ system. The result was due to V_{Zn} as the acceptor, and the donor H_i needs to suppress and compensate for V_{Zn}. Therefore, the hole concentration of the $Zn_{35}SH_iO_{35}$ system decreased. Among the doped systems, the $Zn_{35}SO_{35}$ system had the highest hole concentration of 2.80×10^{21} cm^{-3} and the best conductivity.

3.5. Conductivity analysis

The conductivity calculation formula of a p-type semiconductor is expressed in the literature [39] as the following:

$$\sigma_i = p_i \mu_h e \tag{4}$$

where μ_h and e represent the hole mobility and the amount of elementary charge, respectively. The calculated hole conductivities of all the doped systems along different transport directions are shown in Table 4.

Table 4 shows that the conductivity of the pure $Zn_{36}O_{36}$ system is 0. Compared with the conductivity of the $Zn_{36}O_{36}$ system, the conductivities of the $Zn_{35}SO_{35}$, $Zn_{35}SeO_{35}$, and $Zn_{35}SH_iO_{35}$ systems were remarkably higher. The calculation results showed that the $Zn_{35}SO_{35}$, $Zn_{35}SeO_{35}$, and $Zn_{35}SH_iO_{35}$ systems were all beneficial in terms of improving the conductivity of the ZnO. The com-

Table 4. Conductivities of the $Zn_{36}O_{36}$, $Zn_{35}SO_{35}$, $Zn_{35}SeO_{35}$, and $Zn_{35}SH_iO_{35}$ systems

Models	σ_i (×10^2 S·cm^{-1})	
	G→ F	G→ Z
$Zn_{36}O_{36}$	0	0
$Zn_{35}SO_{35}$	464.39	0.26
$Zn_{35}SeO_{35}$	27.08	0.014
$Zn_{35}SH_iO_{35}$	94.04	474.11

parison of the $Zn_{35}SO_{35}$ and $Zn_{35}SeO_{35}$ systems showed that the conductivity of the S-doped system is remarkably larger than that of the Se-doped system, indicating that S doping is more beneficial in terms of improving the p-type conductivity of ZnO. The comparison of the $Zn_{35}SO_{35}$ and $Zn_{35}SH_iO_{35}$ systems revealed that H_i doping reduces the conductivity of the doped system along the G→ F direction and increases the conductivity of the doped system along the G→ Z direction, indicating that H_i doping can effectively improve the transport performance of the system along the G→ Z direction. Interestingly, in all the doped systems, the conductivities of the $Zn_{35}SO_{35}$ and $Zn_{35}SH_iO_{35}$ systems were the largest along the G→ F and G→ Z directions, respectively.

4. Conclusion

In this paper, the first-principle effects of S/Se/Te doping and the coexistence of V_{Zn} and H_i in ZnO were investigated. The study found that Te doping cannot achieve the p-type degeneracy of the ZnO system, which has no research significance, and S/Se doping is beneficial to the p-type degeneracy of the ZnO system, remarkably improving the hole mobility and electrical conductivity. The $Zn_{35}SO_{35}$, $Zn_{35}SeO_{35}$, and $Zn_{35}SH_iO_{35}$ systems all have good p-type conductivity. Among them, the $Zn_{35}SO_{35}$ system has the highest hole concentration along the G→ F direction at 2.80×10^{21} cm^{-3}, and the best conductivity. The conductivity of the $Zn_{35}SH_iO_{35}$ system was the largest along the G→ Z direction. This result plays a guiding role in obtaining higher-quality p-type ZnO.

Acknowledgements

This work was supported by the National Natural Science Foundation of China (Grant Nos 61664007 and 61964013).

Data Availability Statement

All data that support the findings of this study are included within the article.

References

[1] Dash P, Manna A, Mishrac NC, Varma S. Synthesis and characterization of aligned ZnO nanorods for visible light photocatalysis. *Physica E*. 2019;107: 38–6.

[2] Özgür Ü, Alivov YI, Liu C, Teke A, Reshchikov MA, Doğan S, *et al.* A comprehensive review of ZnO materials and devices. *J Appl Phys*. 2005;98: 041301–103.

[3] Yu W, Xu D, Peng T. Enhanced photocatalytic activity of g-C_3N_4 for selective CO_2 reduction to CH_3OH via facile coupling of ZnO: a direct Z-scheme mechanism. *J Mater Chem*. 2015;3: 19936–47.

[4] Park TY, Choi YS, Kim SM, Jung GY, Park SJ, Kwon BJ, *et al.* Electroluminescence emission from light-emitting diode of p-ZnO/(InGaN/GaN) multiquantum well/n-GaN. *Appl Phys Lett*. 2011;98: 251111–3.

[5] Wang H, Li K, Tao Y, Li J, Li Y, Guo LL, *et al.* Smooth ZnO: Al-AgNWs composite electrode for flexible organic light-emitting device. *Nanoscale Res Lett*. 2017;12: 77–7.

[6] Alfredo BB, Daniel O, Sergio JS. *n*- to *p*-type conductivity transition and band-gap renormalization in ZnO: (Cu+Te) codoped films. *Phys Rev Mater*. 2021;5: 065402–10.

[7] Zhang T, Li MK, Chen J, Wang Y, Miao LS, Lu YM, *et al.* Multi-component ZnO alloys: bandgap engineering, hetero-structures, and optoelectronic devices. *Mater Sci Eng R Rep*. 2022;147: 100661–34.

[8] Niu WZ, Xu HB, Guo YM, Li YG, Ye ZZ, Zhu LP. The effect of sulfur on the electrical properties of S and N co-doped ZnO thin films: experiment and first-principles calculations. *Phys Chem Chem Phys*. 2015;17: 16705–4.

[9] Dib K, Brahimi R, Bessekhouad Y, Tayebi N, Trari M. Structural, optical and transport properties of S_xZnO. *Mater Sci Semicond Process*. 2016;48: 52–9

[10] Cai H, Xu HB, Ye ZZ, Huang JY. Realization of p-type Se–N co-doped ZnO films by radio-frequency magnetron sputtering. *Mater Lett*. 2013;108: 183–5.

[11] Tang K, Gu SL, Wu KP, Zhu SM, Ye JD, Zhang R, *et al.* Tellurium assisted realization of p-type N-doped ZnO. *Appl Phys Lett*. 2010;96: 1830–4.

[12] Park S, Minegishi T, Oh D, Lee H, Taishi T, Park J, *et al.* High-quality p-type ZnO films grown by co-doping of N and Te on Zn-Face ZnO Substrates. *Appl Phys Express*. 2010;3: 031103–3.

[13] Persson C, Platzer-Björkman C, Malmström J, Törndahl T, Edoff M. Strong valence-band offset bowing of $ZnO_{1--x}S_x$ enhances *p*-type nitrogen doping of ZnO-like alloys. *Phys Rev Lett*. 2006;97: 146403–4.

[14] Hou QY, Qi MD, Li Y. Effects of p-type conductive properties of triaxial strain-regulated ZnO (S, Se, Te) system. *Phys Scr*. 2021;96: 125815–11.

[15] Liu YX, Zhang HL, Zhang ZX, Xie YZ, Xie EY. Conversion of p-type to n-type conductivity in undoped ZnO films by increasin operating temperature. *Appl Surf Sci*. 2010;257: 1236–8.

[16] Zeng YJ, Ye ZZ, Xu WZ, Lu JG, He HP, Zhao BH, *et al.* p-type behavior in nominally undoped ZnO thin films by oxygen plasma growth. *Appl Phys Lett*. 2006;88: 262103–3.

[17] Gu T, Hu ET, Guo S, Wu Y, Wang J, Wang ZY, *et al.* Ellipsometric study on optical properties of hydrogen plasma-treated aluminum-doped ZnO thin film. *Vacuum*. 2019;163: 69–74.

[18] Dib K, Brahimi R, Trari M, Bessekhouad Y. Optical properties of S_xZnO and their effect toward the photoacativity. *Optik*. 2019;178: 1102–10.

[19] Welna M, Baranowski M, Linhart WM, Kudrawiec R, Yu KM, Mayer M, *et al.* Multicolor emission from intermediate band semiconductor $ZnO_{1-x}Se_x$. *Sci Rep*. 2017;7: 44214–6.

[20] Sahu R, Dileep K, Negi DS, Nagaraja KK, Datta R. Ambipolar behavior of Te and its effect on the optical emission of ZnO: Te epitaxial thin film. *Phys Status Solidi*. 2015;252: 1743–8.

[21] Wu LQ, Li SQ, Li YC, Li ZZ, Tang GD, Qi WH, *et al.* Presence of monovalent oxygen anions in oxides demonstrated using X-ray photoelectron spectra. *Appl Phys Lett*. 2016;108: 173.

[22] Ghosh S, Khan GG, Das B, Mandal K. Vacancy-induced intrinsic d 0 ferromagnetism and photoluminescence in potassium doped ZnO nanowires. *J Appl Phys*. 2011;109: 951.

[23] Pickett WE, Erwin SC, Ethridge EC. Reformulation of the LDA+U method for a local orbital basis. *Phys Rev B*. 1998;58: 1201–9.

[24] Perdew JP, Burke K, Ernzerhof M. Generalized gradient approximation made simple. *Phys Rev Lett*. 1996;77: 3865–8.

[25] Jia XF, Hou QY, Xu ZC, Qua LF. Effect of Ce doping on the magnetic and optical properties of ZnO by the first principle. *J Magn Magn Mater*. 2018;465: 128–35.

[26] Guo SQ, Hou QY, Zhao CW, Zhang Y. Study of the effect of Cu heavy doping on band gap and absorption spectrum of ZnO. *Chem Phys Lett*. 2014;614: 15–20.

[27] Liu YJ, Hou QY, Sha SL, Xu ZC. Electronic structure, optical and ferromagnetic properties of ZnO co-doped with Ag and Co according to first-principles calculations. *Vacuum*. 2020;173: 109127.

[28] Jaballah S, Benamara M, Dahman H, Ly A, Lahem D, Debliquy M, *et al.* Effect of Mg-doping ZnO nanoparticles on detection of low ethanol concentrations. *Mater Chem Phys*. 2020;255: 123643–11.

[29] Rahm M, Hoffmann R, Ashcroft NW. Atomic and ionic radii of elements 1–96. *Chem Eur J*. 2016;22: 1–9.

[30] Li M, Zhang JY, Zhang Y. First-principles calculation of compensated (2N, W) codoping impacts on band gap engineering in anatase TiO_2. *Chem Phys Lett*. 2012;527: 63–6.

[31] Cui XY, Medvedeva JE, Delley B, Freeman AJ, Newman N, Stampfl C. Role of embedded clustering in dilute magnetic semiconductors: Cr doped GaN. *Phys Rev Lett*. 2005;95: 256404–4

[32] Chris G, Vande W. Interactions of hydrogen with native defects in GaN. *Phys Rev B*. 1997;56: R10 020–23.

[33] Sun PP, Bai LC, Kripalani DR, Zhou K. A new carbon phase with direct bandgap and high carrier mobility as electron transport material for perovskite solarcells. *NPJ Comput Mater*. 2019;5: 1–7.

[34] Deb J, Seriani N, Sarkar U. Ultrahigh carrier mobility of penta-graphene: a first-principle study. *Physica E*. 2021;127: 114507–7.

[35] Hou QY, Sha SL. Effect of biaxial strain on the p-type of conductive properties of (S, Se, Te) and 2 N co-doped ZnO. *Mater Today Commun*. 2020;24: 101063–7.

[36] Janotti A, Van de WalleCG. Fundamentals of zinc oxide as a semiconductor. *Rep Prog Phys*. 2009;72: 126501–29.

[37] Yu WL, Zhang JF, Peng TY. New insight into the enhanced photocatalytic activity of N-, C- and S-doped ZnO photocatalysts. *Appl Catal B: Environ*. 2016;181: 220–7.

[38] Perdew JP, Mel L. Physical content of the exact Kohn–Sham orbital energies: band gap and derivative discontinuities. *Phys Rev Lett*. 1983;51: 1884–7.

[39] Xu ZC, Hou QY, Qu LF. Effects on the optical properties and conductivity of Ag–N co-doped ZnO. *Int J Mod Phys B*. 2017;31: 1750008–18.

Received 2023-01-17
Accepted 2023-02-26